ACS APPLIED MATERIALS & INTERFACES

Research Article

Cite This: ACS Appl. Mater. Interfaces 2018, 10, 5626−5632

www.acsami.org

# Colloidal Quantum Dot Inks for Single-Step-Fabricated Field-Effect Transistors: The Importance of Postdeposition Ligand Removal

Daniel M. Balazs,[†] Nisrina Rizkia,[†] Hong-Hua Fang,[†] Dmitry N. Dirin,[‡,§] Jamo Momand,[†] Bart J. Kooi,[†] Maksym V. Kovalenko,[‡,§] and Maria Antonietta Loi*[,†]

[†]Zernike Institute for Advanced Materials, University of Groningen, Nijenborgh 4, 9747AG Groningen, Netherlands

[‡]Department of Chemistry and Applied Biosciences, ETH Zürich, Vladimir Prelog Weg 1, Zürich 8093, Switzerland

[§]Empa-Swiss Federal Laboratories for Materials Science and Technology, Überlandstrasse 129, Dübendorf 8600, Switzerland

Supporting Information

**ABSTRACT:** Colloidal quantum dots are a class of solution-processed semiconductors with good prospects for photovoltaic and optoelectronic applications. Removal of the surfactant, so-called ligand exchange, is a crucial step in making the solid films conductive, but performing it in solid state introduces surface defects and cracks in the films. Hence, the formation of thick, device-grade films have only been possible through layer-by-layer processing, limiting the technological interest for quantum dot solids. Solution-phase ligand exchange before the deposition allows for the direct deposition of thick, homogeneous films suitable for device applications. In this work, fabrication of field-effect transistors in a single step is reported using blade-coating, an upscalable, industrially relevant technique. Most importantly, a postdeposition washing step results in device properties comparable to the best layer-by-layer processed devices, opening the way for large-scale fabrication and further interest from the research community.

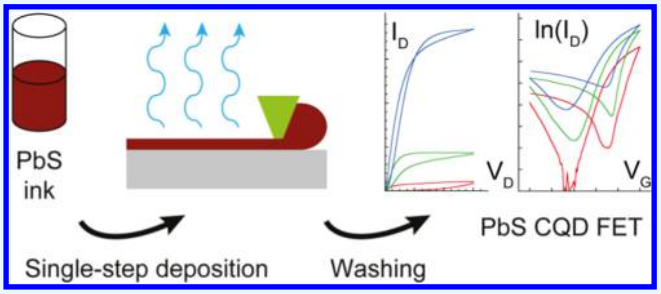


**KEYWORDS:** *colloidal quantum dot, field-effect transistor, colloidal ink, solution-phase ligand exchange, blade-coating*

## INTRODUCTION

Colloidal quantum dot (CQD) solids, arrays of electronically coupled semiconductor nanocrystals, are promising candidates for solution-based fabrication of photovoltaic and optoelectronic devices. Formation of highly conductive films is possible through building up organized and closed-packed assemblies of the CQDs. In the quantum-confined regime, their optical and electronic properties are tunable through the size, the dielectric environment, and the surface properties.[1] Lead-sulfide (PbS) CQDs have been shown to result in >11% photoconversion efficiencies in solar cells,[2] and are also suitable for light-emitting transistors,[3] photodiodes,[4] and logic circuits.[5]

The practical bottleneck in the fabrication process is the difficulty of forming high-quality (i.e., crack-free, dense, ordered) thick arrays in a single step.[1] The as-synthesized CQDs are capped with long, insulating organic ligands that passivate the CQD surface and allow their colloidal dispersion. These ligands need to be removed or exchanged to achieve electronic coupling of the QDs in solids. Such a ligand exchange is usually performed on the QDs that are already assembled in thin film, causing serious cracking and limits to work with rather thin layers, and a layer-by-layer approach is often used to achieve the necessary film thickness and quality.[6−8] In the last decade, a number of methods to perform ligand exchange in the liquid phase before the formation of CQD solids are reported.[9−11] Replacement of the hydrophobic, organic ligands by small, highly charged inorganic ones is accompanied by the migration of the CQDs from the original apolar solvent to a polar one. Chalcogenidometallate complexes, chalcogenides, halides, pseudohalides, and halometallates have been proposed for such processes.[9,12−14] Halides and halometallates show the most prospects for solar cell applications due to the better electronic passivation of the CQD surface.[2,15−17] Field-effect transistors (FETs) based on inorganic-capped PbSe inks have been reported with electron mobilities ranging from 0.03 to 2 $cm^2/(V\ s)$ (depending on the annealing temperature and further surface passivation steps) using spin-coating, a non-upscalable technique only useful in laboratory-scale research.[18,19] Thiocyanate-passivated inks based on larger PbS nanocubes result in 0.1 $cm^2/(V\ s)$ mobility for both electrons and holes, but with a low current modulation.[13] The prospects are clearly enormous, but most works focus only on the materials chemistry of larger, easier-to-handle particles, without much attention on the processability or fine-tuning of the physical properties.

In this work, we aim to fill this gap by studying the electronic properties of the CQD solid films fabricated using a single step and scalable method. We synthesize small-diameter PbS CQD

Received: November 6, 2017
Accepted: January 25, 2018
Published: January 25, 2018




DOI: 10.1021/acsami.7b16882
ACS Appl. Mater. Interfaces 2018, 10, 5626−5632

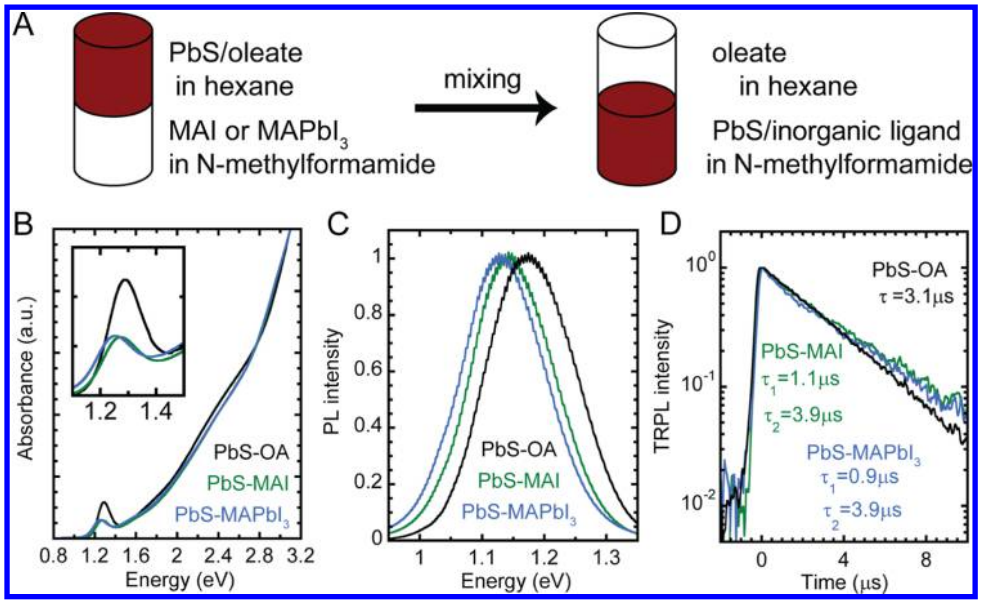


**Figure 1.** (A) Schematic of the solution-phase ligand-exchange process; (B–D) optical absorbance, steady-state photoluminescence (PL) spectra, and PL decay curves of PbS CQD dispersions integrated over the whole peak width.

inks stabilized by inorganic iodide ($I^-$) and iodoplumbate ($PbI_3^-$) complex ligands in a highly polar medium and investigate the quality of the resulting dispersions. We fabricate high-performing field-effect transistors (FETs) by blade-coating and identify the removal of excess ligands as a key step in optimizing the electronic properties of the films. We show the prospects of the approach by achieving 0.12 $cm^2/(V\,s)$ electron mobility and $10^6$ on/off ratio in the FETs fabricated in a single deposition step at mild temperature.

## RESULTS AND DISCUSSION

We prepare halide- and halometallate-stabilized PbS CQD inks following the phase-transfer method developed by Dirin et al. (Figure 1).[9] Two ligand solutions are used: pure methylammonium iodide (MAI) dissolved in *N*-methylformamide (NMF) and a 1:1 mix of MAI and $PbI_2$ also in NMF (hereafter referred to as $MAPbI_3$). The oleate-capped CQDs dispersed in hexane are exposed to the NMF solutions under stirring; successful phase transfer of the CQDs is indicated by bleaching of the apolar phase and darkening of the NMF phase. After purification, the inorganic-capped CQDs are dispersed in propylene carbonate (PC) for film formation. Details of the procedure are found in the Experimental Section.

The absorbance and photoluminescence spectra of the CQD inks are shown in Figure 1B–D, and the extracted peak positions and Stokes-shift values are collected in Table 1. The peak in the absorption spectrum corresponding to the first excitonic transition shows a decreasing maximum intensity, an increasing width, and a mild red-shift upon phase transfer, compared to the oleate-capped CQDs. The broadening can be caused by energy disorder due to varying thickness and composition of the shell. The red-shift can be partially assigned to the different dielectric permittivity ($\varepsilon_r$) of the environment; following the considerations of Takagahara, replacing hexane ($\varepsilon_r$ = 1.9) with PC ($\varepsilon_r$ = 64) by itself can cause a red-shift of several 10 meVs.[20] On the other hand, we see a difference between the peak positions of the two PC dispersions, which may be caused by the different size and dielectric properties of the iodide ion versus the $PbI_3^-$ complex, causing a marginal increase in the effective size of CQDs, and thus a lower confinement in the latter case.

**Table 1. Absorption, Emission Peak Positions, and Stokes Shift for the Original Dispersion and the Formed Inorganic Inks**

| sample | absorption (eV) | emission (eV) | Stokes shift (meV) |
|---|---|---|---|
| PbS–OA/HX | 1.29 | 1.18 | 111 |
| PbS–MAI/PC | 1.27 | 1.15 | 120 |
| PbS–$MAPbI_3$/PC | 1.25 | 1.13 | 125 |

The photoluminescence (PL) spectra show a similar trend as the absorption, without significant broadening. The Stokes shift marginally increases upon ink formation, and is typically around 120 meV. The increased Stokes shift is expected in a highly polar environment, given the higher dipole moment and consequent higher dipolar screening of the excited state in CQDs.[21] Moreover, the energy transfer between CQDs can also cause a shift in the peak position in the presence of a larger disorder. The quality of the samples is further confirmed by measuring the PL decay. Long lifetime in the microsecond range is observed for all three samples. The organic-capped CQDs show a single recombination process with a 3.1 $\mu$s lifetime. The decay becomes slightly biexponential upon ligand exchange, with lifetimes around 1 and 4 $\mu$s, with the latter being the dominant for both samples.

We fabricate FETs based on the CQD inks to test their electronic properties and prospects in practical applications. Details of the film formation and the device structure are listed in the Methods section, and schematics are shown in Figure 2. The CQD films are formed using blade-coating, an upscalable and controllable technique at relatively low (100 °C) temperature. After drying the solvent, the particles appear surrounded by the ligand material (see the transmission electron microscopy (TEM) images in Figure S1a,b), and the films appear smooth and crack-free under atomic force microscopy (AFM) (Figure S1c,d). Both these observations are significantly different from the layer-by-layer processed


DOI: 10.1021/acsami.7b16882
ACS Appl. Mater. Interfaces 2018, 10, 5626–5632

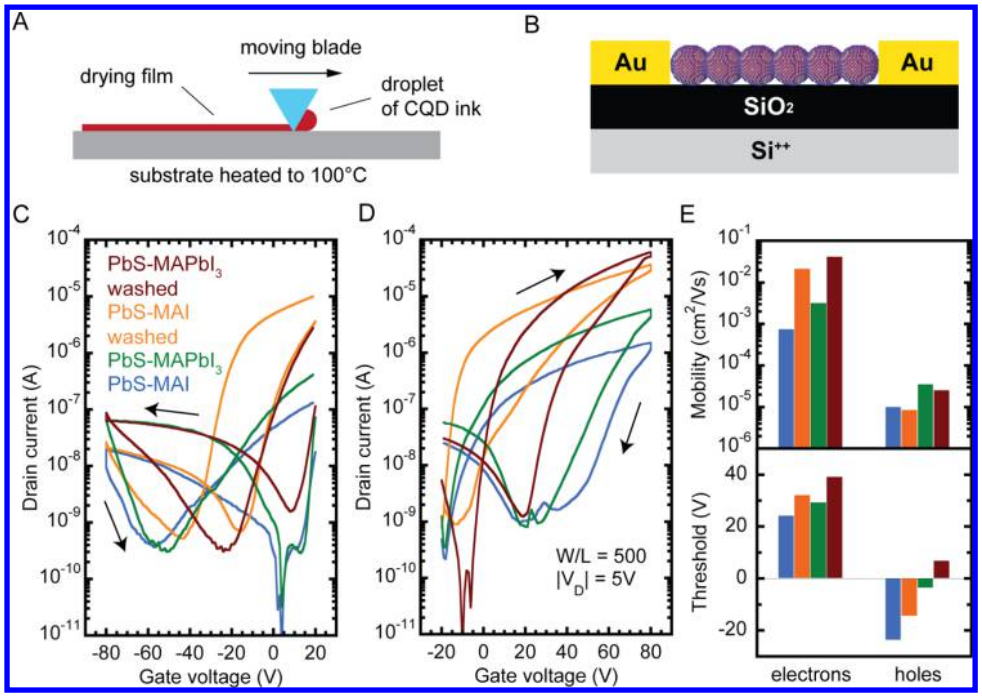


**Figure 2.** PbS CQD FETs based on blade-coated films: schematic of (A) the blade-coating process and (B) the device structure, (C) p-channel and (D) n-channel transfer curves of the PbS−MAI and PbS−$MAPbI_3$ samples before and after washing with methanol, and (E) mobility and threshold values extracted from the transfer curves. The color coding is consistent throughout the figure.

films. Those samples usually exhibit a granular morphology,[6,22,23] and the single CQDs are observable under TEM after the thin-film ligand exchange.[7,24,25]

The transfer curves of the FETs are shown in Figure 2A,B. We observe an electron-dominated ambipolar transistor behavior, namely both electron and hole transport are possible; the p-channel currents (Figure 2A) are, however, orders of magnitude lower than the n-channel ones (Figure 2B). This difference is observed frequently in lead-chalcogenide CQD-based devices and assigned to their stoichiometric imbalance.[25] The general properties are similar to the layer-by-layer processed inorganic-capped PbS CQD solids reported earlier, but the electron currents in the as-deposited films are slightly lower for the same geometry and measurement conditions.[5,7,26] We observe a strong improvement in electron transport upon immersion of the pristine films into pure methanol for 3 min, whereas the hole current remains the same.

We obtain the carrier mobility and threshold voltage values from the linear regime transfer curves using the gradual channel approximation. Electron mobilities around $10^{-3}$ $cm^2/(V\ s)$ are found in the pristine films, which are lower than the literature standards for layer-by-layer processed PbS samples.[5,26] The values improve an order of magnitude with both ligands upon washing using methanol, reaching values exceeding $10^{-2}$ $cm^2/(V\ s)$. On the other hand, the hole mobility does not change after washing the samples and remains around $10^{-5}$ $cm^2/(V\ s)$. Importantly, both electron and hole transport appear to be better in the $MAPbI_3$-treated PbS CQD solids compared to the PbS−MAI samples, which can give a partial explanation to the fact that the complex ligands are shown to work better for the fabrication of efficient solar cells.[27] The obtained mobility values for the washed samples are comparable to those reported earlier in halide-capped PbS CQD solids achieved through layer-by layer postdeposition ligand exchange, showing that similar-quality films can be achieved in a single deposition step using inorganic-capped inks.[7,28,29]

At the same time, both electron and hole threshold voltages shift toward more positive values. The threshold voltage, $V_{th}$, in a thin-film transistor is estimated according to eq 1

$$V_{th} = \phi_{ms} \pm \frac{qn}{C_i} \pm \frac{qNd}{C_i} \quad (1)$$

where $\phi_{ms}$ is the difference in the Fermi levels of the gate metal and semiconductor, $n$ is the trapped charge density in the gate dielectric ($cm^{-2}$), $N$ is the bulk carrier concentration ($cm^{-3}$), and $C_i$ is the gate capacitance ($F\ m^{-2}$).[30] Besides the actual charge carrier concentrations, changes in $\phi_{ms}$ can also cause a threshold shift. The workfunction difference is affected by shifting conduction and valence band energies (relative to the gate contact workfunction) due to surface dipoles at the $SiO_2$ or CQD surface, or changing the Fermi level in the semiconductor (relative to the band edges) through doping. Ionic compounds such as the ligands stabilizing the dispersions can result in significant dipole moments if well-organized at the interface. In CQDs, especially strong shifts in the energy levels up to 2 eV have been observed through dipoles located at the CQD surface,[31−33] and similar range of workfunction shifts are observed in ZnO;[34] but these factors cannot account for the whole threshold shift. Hence, a changing carrier concentration in the CQD film or at the interface is likely the main cause. The two-dimensional charge density difference can be estimated from the values of the variation of the threshold voltage (~10 V for both ligands and both charge carriers), as $\Delta n = C_{ox}\Delta V_{th}/e$ is in the range of $10^{12}$ $cm^{-2}$, or ~0.1 elemental charge per CQD. This carrier density change can be either related to the CQD layer or the $SiO_2$ surface. Assuming a band edge density of states ($N_C$) from the CQD density (~4 nm center-to-center distance in cubic arrangement) to be around $1.6 \times 10^{19}$ $cm^{-3}$,


DOI: 10.1021/acsami.7b16882
ACS Appl. Mater. Interfaces 2018, 10, 5626−5632

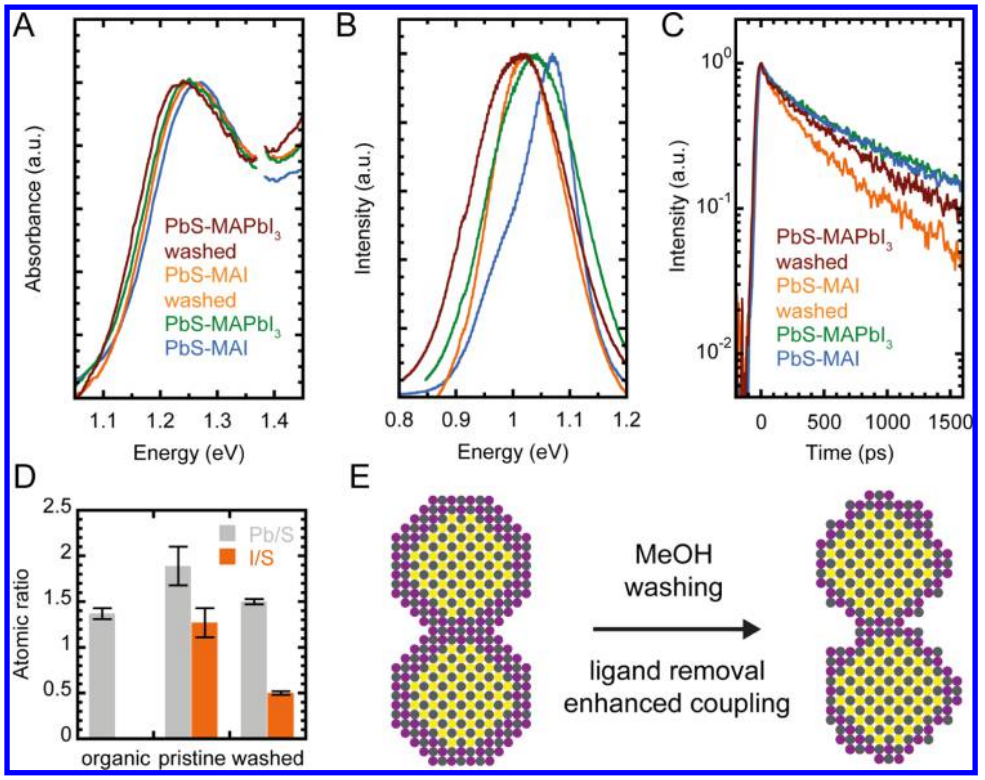


**Figure 3.** (A) Absorbance spectra, (B) steady-state PL spectra, and (C) PL decay of the films prepared from PbS−MAI and PbS−$MAPbI_3$ inks, with and without washing in MeOH; (D) elemental analysis obtained from energy-dispersive X-ray (EDX) data of organic capped PbS and PbS−$MAPbI_3$ CQDs with and without washing; and (E) schematic showing the ligand removal upon washing.

the distance of the Fermi level from the middle of the band gap can be calculated using eq 2

$$\Delta E_F = E_g/2 + kT \ln\left(\frac{N}{N_C}\right) \quad (2)$$

In the presence of $10^{12}$ $cm^{-2}$ charges in the first (~4 nm thick) monolayer from the oxide interface, the Fermi level shifts approximately 0.6 eV from the middle of the band gap. If the carrier sign changes upon washing (e.g., turns from $5 \times 10^{11}$ $cm^{-2}$ of one to the same amount of the other), the Fermi-level shift would be ~1.1 eV. These shifts would alter $\phi_{ms}$ by the same amount; the observed threshold shift is thus mainly stemming from a changing $SiO_2$ surface charge.

We must point out the discrepancy between the direction of the threshold shift and the mobility increase. In an earlier work, we report that air exposure results in a positive threshold shift in PbS CQD FETs; this effect is accompanied by a decrease in the electron mobility, as expected from the underlying trap formation mechanism.[35] Moreover, n-doping the active layer in similar devices results in a negative threshold shift and a higher electron mobility.[26] In this case, however, a positive threshold shift is accompanied by a mobility increase, suggesting that more than a single mechanism should be considered to explain these experimental results.

To explain the observed behavior, we investigate the photophysical properties of the films. The absorbance, steady-state, and time-resolved PL data are shown in Figure 3, and the extracted absorption and PL spectra peak positions and decay lifetimes are listed in Tables S1 and S2, respectively. Interestingly, no red-shift, only a minor broadening, is observed upon film formation (see the direct comparison in Figure S2). However, the peaks show a minor shift of <10 meV toward the lower energies upon washing with MeOH (Figure 3A). Both the PL peak positions and decay lifetimes of the films are different than those of the respective inks. All of the steady-state PL spectra can be fitted with a double Gaussian function, indicating the emission from two distinct states (see Figure S3). A stronger peak is centered around 1.05−1.1 eV, and a weaker one just below 1 eV. In general, washing increases the weight of the lower-energy emission sites, giving an effectively red-shifted emission. The decay curves also show biexponential dynamics, with one lifetime around 100 ps and another in the range of 600−1000 ps. The overall decay becomes faster upon washing, mainly due to the decreased contribution of the slower process, effect stronger in the PbS−MAI thin films. The red-shift and the faster decay are possibly caused by an increased electronic coupling in the film upon washing in MeOH. Moreover, the reduction in the barrier opens more possibilities for non-radiative decay, further decreasing the overall lifetime.

To prove the ligand removal, we determine the layer composition using energy-dispersive X-ray (EDX) spectrometry. We obtained the Pb/S and I/S ratios for the original, oleate-capped CQDs, and the pristine and washed samples prepared using the PbS−$MAPbI_3$ ink (Figure 3D). The original particles show an excess lead, as expected for the synthetic method used. We observe a large amount of iodine and a strong increase in the Pb/S ratio upon phase transfer, showing that we effectively stabilize the PbS−$MAPbI_3$ ink by an iodoplumbate complex attached to the CQD surface.[9] Upon washing with methanol, the Pb/S and I/S ratios both decrease, indicating the partial removal of the capping complex, making the barrier between the CQD cores thinner, more “transparent”.

The overall picture can be interpreted as follows. The lack of the red-shift upon drying indicates that the confinement is not


DOI: 10.1021/acsami.7b16882
ACS Appl. Mater. Interfaces 2018, 10, 5626−5632

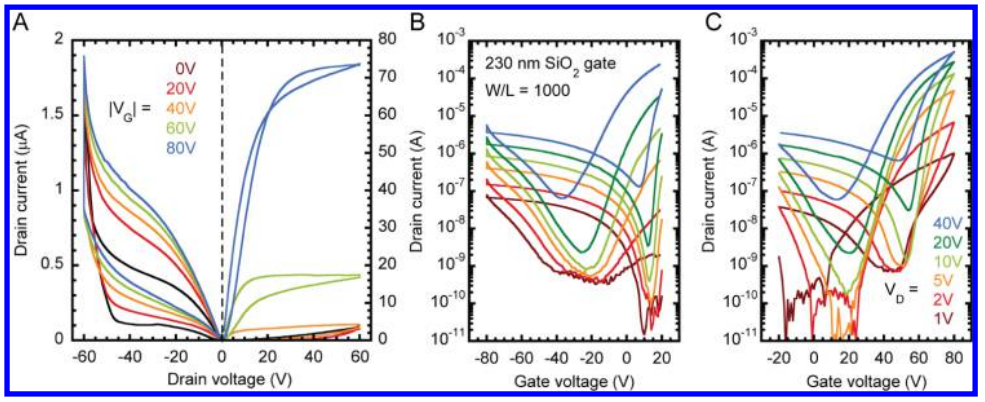


**Figure 4.** Behavior of a representative FET fabricated in a single deposition and washing step using the PbS−$MAPbI_3$ ink: (A) output and (B) p-type and (C) n-type transfer characteristics.

altered by a reduced interdot spacing, and suggests that the ligand shell stabilizing the dispersions prevents significant electronic coupling. This, however, is changed by washing: the red-shift and shorter lifetimes indicate that electronic coupling is induced, or that the trap states become active; both these effects can be caused by washing away of ligands from the CQD surface. The mobility, being limited by single dot-to-dot tunneling events, is strongly dependent on the barrier; hence, the observed increase in mobility suggests that the red-shift is at least partially related to an increase in coupling through the partial removal of the ligand shell. Excess ligands bound to the surface and shielded by a counterion (that make up the stabilizing shell in polar solvents) can cause a shift in the energy levels of the CQDs by forming surface dipoles, uncompensated charges on the CQDs can shift the Fermi-level, and the same ions can also shield the trapped charges at the $SiO_2$ surface. The partial removal of the ligands can thus result in all three previously mentioned effects possibly shifting the threshold in the FETs, but the magnitude of the shift suggests that the $SiO_2$ surface is the main and major origin of it.

By optimizing the substrate treatment and the deposition process, we fabricate high-performing FETs based on the PbS−$MAPbI_3$ ink; the characteristics of a representative device with 10 $\mu$m channel length are shown in Figure 4. Good linear and saturation behavior is observed in the output curves (Figure 4A), with a lower relative hysteresis for electrons than for holes. An injection barrier is observed at room temperature for electrons but not for holes (Figure S3). We measure mobilities up to 0.12 $cm^2/(V\ s)$ for electrons and $10^{-4}$ $cm^2/(V\ s)$ for holes. We observe on/off ratios $>10^6$ in the n-channel and up to $10^3$ in the p-channel. These data are comparable to the best samples fabricated using the conventional layer-by-layer deposition and ligand exchange of the PbS thin films,[5,26] but are now prepared in a single deposition step, confirming the prospects of the solution-phase ligand-exchanged CQD solids for optoelectronic applications.

## CONCLUSIONS

In summary, we show that blade-coating inorganic-capped CQD inks is a facile way to fabricate high-quality thin films and FETs showing performances as good (electron mobility higher than to 0.1 $cm^2/(V\ s)$ and on/off ratios $>10^6$) as the state of the art CQD devices prepared by layer-by-layer solid-state ligand exchange. We show that the as-prepared films contain a large amount of ligands that limit the electron transport, which can be largely improved by a postdeposition washing step. Partial removal of the ligands significantly increases the electron mobility and causes a positive threshold shift, likely by influencing the gate oxide surface. A broader application of these findings could be the next step toward highly efficient solar cells and optoelectronic devices based on colloidal quantum dot solids.

## EXPERIMENTAL SECTION

**Materials.** Lead(II) acetate trihydrate ($PbAc_2{\cdot}3H_2O$, ≥ 99.99%, Aldrich), bis(trimethylsilyl)sulfide ($TMS_2S$, Aldrich), 1-octadecene (ODE, 90%, Aldrich), oleic acid (OA, 90%, Aldrich), ethanol (Fluka), hexane (Aldrich), chloroform (Aldrich), and methanol (Aldrich) were used as received.

**CQD Synthesis.** PbS−OA CQDs were synthesized according to a previously reported method.[36] For the synthesis of 3.1 nm PbS CQDs, a lead precursor solution consisting of 1.5 g $PbAc_2{\cdot}3H_2O$ in 47 mL ODE and 2.8 mL OA was vacuum dried for an hour at 120 °C in a three-neck reaction flask. The atmosphere was then switched to argon and the temperature was subsequently changed to 105 °C. After that, the heating mantle was removed and a sulfur precursor of 420 $\mu$L $TMS_2S$ in 10 mL of dried ODE was quickly injected. After 3 min of growth, the flask was cooled down to room temperature by an ice bath. Hexane (39 mL) and ethanol (102 mL) were added to the crude solution, followed by centrifugation to separate the CQDs. Two more washing steps were performed by redispersion in hexane (39 and 18 mL on the first and second washing steps, respectively) and precipitation by ethanol (45 and 21 mL, respectively). One extra washing step was performed by the redispersion CQDs in 3 mL chloroform and precipitation by 3 mL methanol. The final pellet was dissolved in 4 mL of anhydrous chloroform and filtered through 450 $\mu$m poly(tetrafluoroethylene) filter. The particles were dried in mild vacuum and dispersed in hexane at the required concentration before ligand exchange.

**Ligand Exchange.** Phase transfer into a polar solvent by ligand exchange was performed by exposing the apolar dispersions to a polar solvent containing the inorganic ligands. In a typical procedure, 10 mL of oleate-capped PbS CQDs dispersed in hexanes (~5 mg/mL) was poured on top 10 mL of a 50 mM MAI or $MAI/PbI_2$ (1:1) solution in NMF. The mixture was stirred at 700−1000 rpm (mild stirring, vortex visible) for 12−24 h, leading to the phase transfer of PbS QDs from the nonpolar to the polar phase, resulting in a colorless top phase. The top phase was removed by a syringe and the bottom phase was rinsed three times with hexane (10 mL of hexane each time, vigorously stirred for ~10 min). The inorganic-capped CQDs were precipitated by adding 10 mL acetone (and a couple droplets of toluene in case it is necessary) and left to settle for 1−2 h. The solution was completely separated by centrifuging at 16 000 rpm for 15 minutes. The supernatant was removed and the pellet redispersed in propylene carbonate at 50−100 mg/mL concentration.


DOI: 10.1021/acsami.7b16882
ACS Appl. Mater. Interfaces 2018, 10, 5626−5632

**FET Fabrication.** Substrates for thin films were cleaned by sonication in acetone and isopropyl alcohol and treated by ozone or vacuum plasma treatment, or longer annealing in inert atmosphere for good wetting. For FETs, 5−40 nm films were formed on $Si^{++}/SiO_2$ (230 nm) substrates carrying the electrode pattern (10 nm indium tin oxide/30 nm Au) by blade-coating of the PC-based inks. Lithographically defined interdigitated electrodes forming channels 10 or 20 $\mu$m long and 1 cm wide were used. In a typical procedure, 3 $\mu$L of the (previously stirred) ink was injected between the blade and the substrate (with a gap of 10 $\mu$m) on a table heated to 100 °C. The droplet was spread by moving the blade across the substrate at 50 mm/s speed, and the film was left dry on the table. The washing was performed in a Petri dish by immersion for 3 min at room temperature. The fabrication was finalized by annealing the samples at 120 °C for 20 min. The samples for absorption and photoluminescence measurements were drop-cast on quartz substrates at the thicknesses of around 100 nm and treated the same way. All of the fabrication steps were performed in inert atmosphere (<0.1 ppm $H_2O/O_2$).

**Film Characterization.** The absorbance spectra were collected using a Shimadzu UV-3000 UV/vis/near-infrared (NIR) spectrometer. For the steady-state and time-integrated photoluminescence (PL) measurements, the second harmonic (3.1 eV) from a mode-locked Ti:sapphire laser (Mira 900, Coherent) was used as excitation source. The laser power was adjusted using neutral-density filters to 0.3 mW (solutions) or 3 mW (thin films). The excitation beam was spatially limited by an iris and focused with a 150 mm focal length lens. The PL was collected into a spectrometer and recorded by Andor 1.7 $\mu$m InGaAs camera. The time-resolved PL spectra were dispersed by an imaging spectrometer and detected using a Hamamatsu NIR streak camera. For the thin-film lifetime, the streak camera was operated in the synchroscan mode with the time resolution of around 10 ps. For the PL lifetime of the OA-capped samples, a slow-single-sweep unit was used and a pulse picker was employed to reduce the repetition rate of the exciting pulses. The FETs were characterized using an Agilent 5262A Semiconductor Parameter Analyzer in a nitrogen-filled glovebox (<0.1 ppm $H_2O/O_2$). Differential transconductance and threshold values were extracted from the forward (away from 0 V) scanned branch of transfer curves measured at ±5 V drain bias. Mobilities were calculated from the differential transconductances based on the gradual channel approximation.[37] The AFM images were obtained using a WITec $\alpha$ SNOM-AFM. The TEM and EDX data were collected from samples drop-cast on carbon-coated copper grids using a JEOL 2010, equipped with a $LN_2$-cooled SiLi detector at 200 kV. The spectra were fitted with the Cliff−Lorimer (MBTS) correction method w/o absorbance, as implemented in the NSS 2.3 software package from Thermo Scientific.

## ■ ASSOCIATED CONTENT

### Supporting Information

The Supporting Information is available free of charge on the ACS Publications website at DOI: 10.1021/acsami.7b16882.

TEM and AFM images, additional photoluminescence, and FET data (PDF)

## ■ AUTHOR INFORMATION


### Corresponding Author

*E-mail: m.a.loi@rug.nl.

### ORCID

Daniel M. Balazs: 0000-0001-7597-043X
Dmitry N. Dirin: 0000-0002-5187-4555
Maksym V. Kovalenko: 0000-0002-6396-8938
Maria Antonietta Loi: 0000-0002-7985-7431


### Author Contributions

D.M.B. and M.A.L. designed the project, D.N.D. synthesized the quantum dots, D.M.B. and N.R. optimized the recipe and formed the films, H.-H.F performed the photoluminescence measurements, J.M. obtained the EDX data and the TEM images. The different parts of the experimental work were supervised by B.J.K., M.V.K., and M.A.L. The manuscript was written by D.M.B and M.A.L., with contribution from the other authors. All of the authors have given approval to the final version of the manuscript.

### Notes

The authors declare no competing financial interest.

## ■ ACKNOWLEDGMENTS

The authors express their gratitude to A. Kamp, T. Zaharia, and G. ten Brink for the technical assistance. The work was funded by the European Research Council through ERC Starting Grants "HySPOD" No. 306983 (D.M.B., H.-H.F., and M.A.L.) and "Nanosolid" No. 306733 (D.N.D. and M.V.K.), and the Swiss Federal Commission for Technology and Innovation through the grant CTI-Nos. 18614.1; 25493.3 (D.N.D. and M.V.K.).

## ■ REFERENCES


(1) Kagan, C. R.; Murray, C. B. Charge transport in strongly coupled quantum dot solids. *Nat. Nanotechnol.* **2015**, *10*, 1013−1026.

(2) Liu, M.; Voznyy, O.; Sabatini, R.; de Arquer, F. P. G.; Munir, R.; Balawi, A. H.; Lan, X.; Fan, F.; Walters, G.; Kirmani, A. R.; Hoogland, S.; Laquai, F.; Amassian, A.; Sargent, E. H. Hybrid organic−inorganic inks flatten the energy landscape in colloidal quantum dot solids. *Nat. Mater.* **2017**, *16*, 258−263.

(3) Schornbaum, J.; Zakharko, Y.; Held, M.; Thiemann, S.; Gannott, F.; Zaumseil, J. Light-emitting quantum dot transistors: emission at high charge carrier densities. *Nano Lett.* **2015**, *15*, 1822−1828.

(4) Jarzab, D.; Szendrei, K.; Yarema, M.; Pichler, S.; Heiss, W.; Loi, M. A. Charge-Separation Dynamics in Inorganic−Organic Ternary Blends for Efficient Infrared Photodiodes. *Adv. Funct. Mater.* **2011**, *21*, 1988−1992.

(5) Shulga, A. G.; Derenskyi, V.; Salazar-Rios, J. M.; Dirin, D. N.; Fritsch, M.; Kovalenko, M. V.; Scherf, U.; Loi, M. A. An All-Solution-Based Hybrid CMOS-Like Quantum Dot/Carbon Nanotube Inverter. *Adv. Mater.* **2017**, *29*, No. 1701764.

(6) Bisri, S. Z.; Piliego, C.; Yarema, M.; Heiss, W.; Loi, M. A. Low Driving Voltage and High Mobility Ambipolar Field-Effect Transistors with PbS Colloidal Nanocrystals. *Adv. Mater.* **2013**, *25*, 4309−4314.

(7) Balazs, D. M.; Dirin, D. N.; Fang, H.-H.; Protesescu, L.; ten Brink, G. H.; Kooi, B. J.; Kovalenko, M. V.; Loi, M. A. Counterion-Mediated Ligand Exchange for PbS Colloidal Quantum Dot Superlattices. *ACS Nano* **2015**, *9*, 11951−11959.

(8) Speirs, M. J.; Dirin, D. N.; Abdu-Aguye, M.; Balazs, D. M.; Kovalenko, M. V.; Loi, M. A. Temperature dependent behaviour of lead sulfide quantum dot solar cells and films. *Energy Environ. Sci.* **2016**, *9*, 2916−2924.

(9) Dirin, D. N.; Dreyfuss, S.; Bodnarchuk, M. I.; Nedelcu, G.; Papagiorgis, P.; Itskos, G.; Kovalenko, M. V. Lead Halide Perovskites and Other Metal Halide Complexes As Inorganic Capping Ligands for Colloidal Nanocrystals. *J. Am. Chem. Soc.* **2014**, *136*, 6550−6553.

(10) Dolzhnikov, D. S.; Zhang, H.; Jang, J.; Son, J. S.; Panthani, M. G.; Shibata, T.; Chattopadhyay, S.; Talapin, D. V. Composition-matched molecular "solders" for semiconductors. *Science* **2015**, *347*, 425−428.

(11) Zhang, H.; Dasbiswas, K.; Ludwig, N. B.; Han, G.; Lee, B.; Vaikuntanathan, S.; Talapin, D. V. Stable colloids in molten inorganic salts. *Nature* **2017**, *542*, 328−331.

(12) Kovalenko, M. V.; Scheele, M.; Talapin, D. V. Colloidal Nanocrystals with Molecular Metal Chalcogenide Surface Ligands. *Science* **2009**, *324*, 1417−1420.

(13) Koh, W.-k.; Saudari, S. R.; Fafarman, A. T.; Kagan, C. R.; Murray, C. B. Thiocyanate-capped PbS Nanocubes: Ambipolar




DOI: 10.1021/acsami.7b16882
*ACS Appl. Mater. Interfaces* 2018, 10, 5626−5632

Transport Enables Quantum Dot Based Circuits on a Flexible Substrate. *Nano Lett.* **2011**, *11*, 4764−4767.
(14) Zhang, H.; Jang, J.; Liu, W.; Talapin, D. V. Colloidal Nanocrystals with Inorganic Halide, Pseudohalide, and Halometallate Ligands. *ACS Nano* **2014**, *8*, 7359−7369.
(15) Ning, Z.; Dong, H.; Zhang, Q.; Voznyy, O.; Sargent, E. H. Solar Cells Based on Inks of n-Type Colloidal Quantum Dots. *ACS Nano* **2014**, *8*, 10321−10327.
(16) Kim, S.; Noh, J.; Choi, H.; Ha, H.; Song, J. H.; Shim, H. C.; Jang, J.; Beard, M. C.; Jeong, S. One-Step Deposition of Photovoltaic Layers Using Iodide Terminated PbS Quantum Dots. *J. Phys. Chem. Lett.* **2014**, *5*, 4002−4007.
(17) Zhang, X.; Zhang, J.; Phuyal, D.; Du, J.; Tian, L.; Öberg, V. A.; Johansson, M. B.; Cappel, U. B.; Karis, O.; Liu, J.; Rensmo, H.; Boschloo, G.; Johansson, E. M. J. Inorganic $CsPbI_3$ Perovskite Coating on PbS Quantum Dot for Highly Efficient and Stable Infrared Light Converting Solar Cells. *Adv. Energy Mater.* **2017**, No. 1702049.
(18) Sayevich, V.; Gaponik, N.; Plötner, M.; Kruszynska, M.; Gemming, T.; Dzhagan, V. M.; Akhavan, S.; Zahn, D. R. T.; Demir, H. V.; Eychmüller, A. Stable Dispersion of Iodide-Capped PbSe Quantum Dots for High-Performance Low-Temperature Processed Electronics and Optoelectronics. *Chem. Mater.* **2015**, *27*, 4328−4337.
(19) Lin, Q.; Yun, H. J.; Liu, W.; Song, H.-J.; Makarov, N. S.; Isaienko, O.; Nakotte, T.; Chen, G.; Luo, H.; Klimov, V. I.; Pietryga, J. M. Phase-transfer ligand exchange of lead chalcogenide quantum dots for direct deposition of thick, highly conductive films. *J. Am. Chem. Soc.* **2017**, *139*, 6644−6653.
(20) Takagahara, T. Effects of dielectric confinement and electron−hole exchange interaction on excitonic states in semiconductor quantum dots. *Phys. Rev. B* **1993**, *47*, No. 4569.
(21) Sargent, E. H.; Klem, E. J. D.; Levina, L. PbS quantum dot electroabsorption modulation across the extended communications band 1200−1700 nm. *Appl. Phys. Lett.* **2005**, *87*, No. 053101.
(22) Nugraha, M. I.; Häusermann, R.; Bisri, S. Z.; Matsui, H.; Sytnyk, M.; Heiss, W.; Takeya, J.; Loi, M. A. High Mobility and Low Density of Trap States in Dual-Solid-Gated PbS Nanocrystal Field-Effect Transistors. *Adv. Mater.* **2015**, *27*, 2107−2112.
(23) Shulga, A. G.; Piveteau, L.; Bisri, S. Z.; Kovalenko, M. V.; Loi, M. A. Double Gate PbS Quantum Dot Field-Effect Transistors for Tuneable Electrical Characteristics. *Adv. Electron. Mater.* **2016**, *2*, No. 1500467.
(24) Speirs, M. J.; Balazs, D. M.; Fang, H.-H.; Lai, L.-H.; Protesescu, L.; Kovalenko, M. V.; Loi, M. A. Origin of the Increased Open Circuit Voltage in PbS−CdS Core−Shell Quantum Dot Solar Cells. *J. Mater. Chem. A* **2015**, *3*, 1450−1457.
(25) Balazs, D. M.; Bijlsma, K. I.; Fang, H.-H.; Dirin, D. N.; Döbeli, M.; Kovalenko, M. V.; Loi, M. A. Stoichiometric control of the density of states in PbS colloidal quantum dot solids. *Sci. Adv.* **2017**, *3*, No. eaao1558.
(26) Nugraha, M. I.; Kumagai, S.; Watanabe, S.; Sytnyk, M.; Heiss, W.; Loi, M. A.; Takeya, J. Enabling Ambipolar to Heavy n-Type Transport in PbS Quantum Dot Solids through Doping with Organic Molecules. *ACS Appl. Mater. Interfaces* **2017**, *9*, 18039−18045.
(27) Yang, Z.; Janmohamed, A.; Lan, X.; de Arquer, F. P. G.; Voznyy, O.; Yassitepe, E.; Kim, G.-H.; Ning, Z.; Gong, X.; Comin, R.; Sargent, E. H. Colloidal Quantum Dot Photovoltaics Enhanced by Perovskite Shelling. *Nano Lett.* **2015**, *15*, 7539−7543.
(28) Zhitomirsky, D.; Furukawa, M.; Tang, J.; Stadler, P.; Hoogland, S.; Voznyy, O.; Liu, H.; Sargent, E. H. N-Type Colloidal-Quantum-Dot Solids for Photovoltaics. *Adv. Mater.* **2012**, *24*, 6181−6185.
(29) Oh, S. J.; Wang, Z.; Berry, N. E.; Choi, J.-H.; Zhao, T.; Gaulding, E. A.; Paik, T.; Lai, Y.; Murray, C. B.; Kagan, C. R. Engineering Charge Injection and Charge Transport for High Performance PbSe Nanocrystal Thin Film Devices and Circuits. *Nano Lett.* **2014**, *14*, 6210−6216.
(30) Horowitz, G.; Hajlaoui, R.; Bouchriha, H.; Bourguiga, R.; Hajlaoui, M. The Concept of "Threshold Voltage" in Organic Field-Effect Transistors. *Adv. Mater.* **1998**, *10*, 923−927.
(31) Soreni-Harari, M.; Yaacobi-Gross, N.; Steiner, D.; Aharoni, A.; Banin, U.; Millo, O.; Tessler, N. Tuning energetic levels in nanocrystal quantum dots through surface manipulations. *Nano Lett.* **2008**, *8*, 678−684.
(32) Brown, P. R.; Kim, D.; Lunt, R. R.; Zhao, N.; Bawendi, M. G.; Grossman, J. C.; Bulović, V. Energy level modification in lead sulfide quantum dot thin films through ligand exchange. *ACS Nano* **2014**, *8*, 5863−5872.
(33) Kroupa, D. M.; Vörös, M.; Brawand, N. P.; McNichols, B. W.; Miller, E. M.; Gu, J.; Nozik, A. J.; Sellinger, A.; Galli, G.; Beard, M. C. Tuning colloidal quantum dot band edge positions through solution-phase surface chemistry modification. *Nat. Commun.* **2017**, *8*, No. 15257.
(34) Lange, I.; Reiter, S.; Pätzel, M.; Zykov, A.; Nefedov, A.; Hildebrandt, J.; Hecht, S.; Kowarik, S.; Wöll, C.; Heimel, G.; Neher, D. Tuning the Work Function of Polar Zinc Oxide Surfaces using Modified Phosphonic Acid Self-Assembled Monolayers. *Adv. Funct. Mater.* **2014**, *24*, 7014−7024.
(35) Balazs, D. M.; Nugraha, M. I.; Bisri, S. Z.; Sytnyk, M.; Heiss, W.; Loi, M. A. Reducing Charge Trapping in PbS Colloidal Quantum Dot Solids. *Appl. Phys. Lett.* **2014**, *104*, No. 112104.
(36) Hines, M. A.; Scholes, G. D. Colloidal PbS Nanocrystals with Size-Tunable Near-Infrared Emission: Observation of Post-Synthesis Self-Narrowing of the Particle Size Distribution. *Adv. Mater.* **2003**, *15*, 1844−1849.
(37) Sze, S. M.; Kwok, K. N. *Physics of Semiconductor Devices*; Wiley-Interscience: Hoboken, NJ, 2007.


DOI: 10.1021/acsami.7b16882
*ACS Appl. Mater. Interfaces* 2018, 10, 5626−5632